

Journal of Applied Remote Sensing

RemoteSensing.SPIEDigitalLibrary.org

Attribution of local climate zones using a multitemporal land use/land cover classification scheme

Andreas Wicki
Eberhard Parlow

SPIE.

Andreas Wicki, Eberhard Parlow, "Attribution of local climate zones using a multitemporal land use/land cover classification scheme," *J. Appl. Remote Sens.* **11**(2), 026001 (2017), doi: 10.1117/1.JRS.11.026001.

Attribution of local climate zones using a multitemporal land use/land cover classification scheme

Andreas Wicki* and Eberhard Parlow

University of Basel, Faculty of Science, Department of Environmental Sciences, Research Group of Meteorology, Climatology and Remote Sensing, Basel, Switzerland

Abstract. Worldwide, the number of people living in an urban environment exceeds the rural population with increasing tendency. Especially in relation to global climate change, cities play a major role considering the impacts of extreme heat waves on the population. For urban planners, it is important to know which types of urban structures are beneficial for a comfortable urban climate and which actions can be taken to improve urban climate conditions. Therefore, it is essential to differ between not only urban and rural environments, but also between different levels of urban densification. To compare these built-up types within different cities worldwide, Stewart and Oke developed the concept of local climate zones (LCZ) defined by morphological characteristics. The original LCZ scheme often has considerable problems when adapted to European cities with historical city centers, including narrow streets and irregular patterns. In this study, a method to bridge the gap between a classical land use/land cover (LULC) classification and the LCZ scheme is presented. Multitemporal Landsat 8 data are used to create a high accuracy LULC map, which is linked to the LCZ by morphological parameters derived from a high-resolution digital surface model and cadastral data. A bijective combination of the different classification schemes could not be achieved completely due to overlapping threshold values and the spatially homogeneous distribution of morphological parameters, but the attribution of LCZ to the LULC classification was successful. © The Authors. Published by SPIE under a Creative Commons Attribution 3.0 Unported License. Distribution or reproduction of this work in whole or in part requires full attribution of the original publication, including its DOI. [DOI: [10.1117/1.JRS.11.026001](https://doi.org/10.1117/1.JRS.11.026001)]

Keywords: local climate zones; land use/land cover; Landsat 8; morphology; urban.

Paper 160978 received Dec. 22, 2016; accepted for publication Mar. 15, 2017; published online Apr. 3, 2017.

1 Introduction

Before the use of air conditioning to counteract unpleasant effects of enhanced heat stress, people used to construct their housing adapted to the local climate conditions. This kind of urban architecture can still be observed in old Arabic medina districts¹ or in the historical centers of European cities. Modern urban design, however, often ignored its role in the urban climate system due to improved heating and cooling systems. During periods of rapid climate change,² these adaptations have to be reinvented, especially in the moderate and temperate climate zones.

Historical centers define usually the core of most European or North African cities with different morphology due to climatic differences, topographic adaption, demographic and cultural development, and destruction through totalitarian regimes³ or wars. Comparing buildings outside the old medieval core built over the last 200 years during rapid urban growth (i.e., Wilhelminian or Gruenderzeit era) with suburban neighborhoods, urban morphological characteristics like street width, mean building height, or building density differ substantially. These differences are well observable in satellite imagery with subkilometer resolution or in orthophotos. The major challenge of land surface analysis is to translate these visible differences into comprehensible quantities. Although satellite sensors usually measure data in a spectral range beyond the visible wavelengths, and therefore see many more differences than the

*Address all correspondence to: Andreas Wicki, E-mail: a.wicki@unibas.ch

human eye, they cannot classify surface structures automatically. Different approaches of characterizing these measurements have been developed: One possibility is to work with different indices to identify and quantify vegetation,^{4,5} soil,⁶ buildings,^{7,8} and water bodies.⁹ Spectral mixture analysis^{10–12} and support vector regression,¹³ to estimate the composition of satellite imagery, are other popular methods. In this study, a classical approach using a maximum-likelihood classification based on ground truth data [regions of interest (ROIs)] is used to subdivide the city into different levels of densification with various characteristics concerning thermal behavior, air movement, morphological parameters, vegetation cover, and many more. This information is crucial for urban development and should be available to planners in a useful manner to enable the distribution of knowledge about basic urban climate aspects among the different disciplines.^{14–16} Furthermore, LULC analysis data are important for urban climate scientists as an input for models and urban climate studies.

Another issue of land surface analysis is the comparability of different classification schemes throughout different cities around the world.^{17–23} Stewart and Oke¹⁷ have tried to overcome this heterogeneity concerning land cover analyses with their local climate zones (LCZ) classification scheme. The major thinking behind this approach is the definition of general zones within cities in different countries worldwide to compare the climatic behavior. This can be very useful, for example, to characterize the urban environment of a meteorological measurement station. The idea of subdividing cities into “climate zones” has a long tradition in urban climatology. Weischet introduced his *Baukörperklimatologie* (building-complex climatology) to group similar urban structures and investigate their influence on the local climate of Freiburg im Breisgau in the 1970s.^{24,25} Scherer et al.²³ defined “climatopes” and Fehrenbach²⁶ so-called “areal types,” which already considered fractions of different land cover in a satellite pixel.

The LCZ approach claims to be universal and applicable in cities all over the world. It is based on morphological parameters like imperviousness (impervious surface fraction and pervious surface fraction), sky view factor, height of roughness elements (buildings and vegetation, here referred to as mean building height), building to surface fraction, and aspect ratio. This scheme is used by many scientists in current research as a common reference frame and has a certain impact on urban climate science, as it is frequently applied by the urban climate community.^{18,27–29} But many people overestimated the fact that the scheme does not cover the heterogeneity in an old European city as easily as the chessboard-structure of a planned North American city. Using the thresholds of the LCZ scheme in a strict manner results in many unclassified areas and only in a few different LCZ classes.²⁹ Altering the thresholds on the other hand would reduce the comparability, which is one of the major advantages of the LCZ classification. Often, the only way to generate comprehensive LCZ is to map them manually. Nevertheless, the LCZ scheme offers the possibility to compare different parts of different cities with trenchant distinctions representing the heterogeneous thermal behavior within an urban environment.

To use the benefits of the LCZ scheme and apply them to a classical LULC classification, a method to bridge the gap between those different approaches has been developed. The following sections describe the workflow of this simple way to merge different classification schemes.

2 Materials and Methods

2.1 Site Description

The city of Basel is located in the southern part of the Upper Rhine Valley in the trinational border region France–Germany–Switzerland and is the capital of the Canton Basel-Stadt (BS). The city structure is characterized by the river Rhine, whose channel undergoes an almost 90 deg bend during its passage through the city to enter the upper Rhine valley in the north (Fig. 1).

Basel is well known for its historical old town center located on the south bank of the river with a minor part on the north bank. Large industrial areas hosting big pharmaceutical/chemical companies along the river are sited at the eastern and northwestern borders of the city. Compared

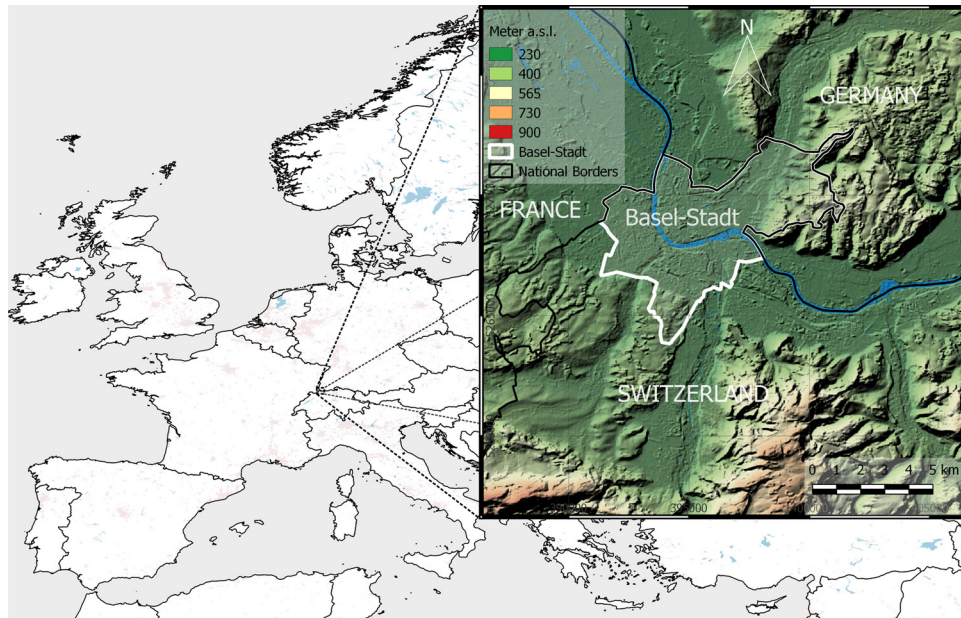


Fig. 1 Overview and location of the study area (map extent) with a topographic map based on the Aster GDEM data set including the borders of the Canton Basel-Stadt (white) and the surrounding countries (black) as a vector overlay. The overview map is created with Natural Earth data.³⁰

to other Swiss cities, Basel (250 m a.s.l.) has a relatively mild climate with record high summer temperatures. The annual mean temperature is 10.5°C with an annual precipitation of 842 mm according to the suburban weather station Basel/Binningen maintained by the Federal Office of Meteorology and Climatology (MeteoSwiss) for the reference period 1981 to 2010.³¹ Although the city is located between the mountains of Jura, Vosges, and Black Forest providing the city with fresh air,²³ the distinct nocturnal urban heat island causes severe heat stress during major heat waves.^{32,33}

The investigation area contains the metropolitan area of Basel with ~730,000 inhabitants in total including the bordering suburbs located in the Canton Basel-Land (BL), the German cities Weil am Rhein and Lörrach, the French city Saint-Louis and the city of Basel.¹⁵ The north to south and west to east extent reaches 21 by 20 km², respectively, spanning from the upper left 47°38'35"N 7°29'17"E to the lower right 47°27'25"N 7°45'32"E.

2.2 Data

For this study, Landsat 8 data acquired between June and August 2013 to 2015 with a minimum cloud and haze cover is used from the Landsat paths 195/196 and row 27. Seven cloud free scenes with a comparable sun elevation were selected as an input for the classification algorithm.

Morphological parameters are estimated by rasterizing a digital surface model (DSM) provided by the administration of BS³⁴ updated with LIDAR derived tree information and vector data of the official cadastral survey to a 1-m raster grid.³⁴ Typical for an international border zone, these data are only available for BS (white polygon in Fig. 1), omitting the French, the German, and the BL parts (Table 1).

2.3 Methods

2.3.1 Land use/land cover

The LULC map is created using multitemporal Landsat 8 images in the VIS, NIR, and SWIR range. Additionally, the data are resampled to 15 m using the Gram–Schmidt pan-sharpening

Table 1 Raster and original vector datasets used in this study with corresponding acquisition or update time.

	Dataset	Acquisition date/last update
Raster	Landsat 8 OLI	05 June 2013, 08 June 2014, 17 July 2014, 11 June 2015, 04 July 2015, 05 August 2015, 30 August 2015
Vector (origin)	Administrative boundaries	Downloaded 23 February 2016
	Official cadastral survey	Downloaded 04 March 2016
	DSM	Validity 20 March 2009
	LIDAR-derived trees	Validity 19 November 2011
	Communal boundaries	Downloaded 26 January 2016

algorithm. Therefore, a higher spatial resolution panchromatic image is merged with several lower resolution bands using a statistical procedure.³⁵ Especially considering the sharpness, Gram–Schmidt pan-sharpening is known for generally high quality results.³⁶ Although theoretically pixel-based classifications are not applicable on pan-sharpened images, particular tests have shown higher accuracy compared to the 30-m original data (see Sec. 4.1 for more information).

The LULC analysis is based on a supervised classification using ROIs as training areas for a maximum-likelihood algorithm.^{37,38} After several runs and refining of the training areas to reduce the unclassified and false classified pixels, the same ROIs are used to calculate the maximum-likelihood for six other Landsat 8 images covering the same extent and satisfying the criteria (no clouds, no haze, high sun elevation, and comparable vegetation cover). In a next step, the classification images are stacked and combined expecting that not all pixels in the various Landsat 8 images were classified in the same way. Thereafter, every individual pixel in the final product is the result of the most frequently occurring class (i.e., modal value) of the specific x - y -location in the different classification layers among this multilayer stack. A similar approach was used before to successfully create complete coverage land cover maps with improved accuracy of areas with high cloud frequency.³⁹

Unclassified pixels are omitted and filled with the class-majority of the neighboring pixels. This is done first in a 3×3 surrounding and, if unclassified pixels still occur, in a 5×5 surrounding.

This procedure is applied only for the built-up classes and the water class, where no—or only minor—changes are expected within the two-and-a-half-year period. Due to the heterogeneity of the surrounding landscapes and the urban material, 25 different ROIs and resulting classes are determined. Finally, these classes are grouped reasonably in five different nonurban and six built-up classes due to the structures of the city and their natural surroundings (Table 2). Most of the grouping concerned the classes forest, water, agriculture green, and agriculture yellow, which represented a large number of the 25 ROIs.

2.3.2 Morphological parameters

The morphological parameters are estimated using GIS data provided by the administration of BS. Therefore, the data are spatially limited by the borders of BS (see Fig. 1 for orientation).

The sky view factor is calculated using the urban multiscale environmental predictor (UMEP), an extension to QGIS provided by Lindberg et al.⁴⁰ To reduce computation time, the building layer of the vector DSM is rasterized to 3 m. Urban trees, received from LIDAR data provided by the administration of BS, are added for the sky view factor calculations as well. The values of roof and vegetation pixels are masked to obtain the ground-level sky view factor product.

Table 2 Description of the final LULC class compositions considering real world conditions after combination and filtering.

Class	Description
Dense Urban	Preindustrial old town development, small houses, roof tiles, crooked and narrow streets, minimum vegetation cover
Urban	Wilhelminian housing with regular three to five story buildings and backyards with greenspace
Suburban	Detached/semidetached houses with gardens, two to three story buildings
Urban Garden	Allotment gardens, cemeteries
Rail/Road/Concrete	Large roads, open concrete space, train stations, bridges, large railways, railway sidings
Industry/Commercial	Manufactories, metal roofs, industrial neighborhoods, port, construction sites, artificial sports ground, pharmaceutical/chemical industry
Agriculture Yellow	Mature crops, rape
Agriculture Green	Meadows, growing crops, maize, urban greenspace
Vineyard/Shrub	Vineyards, shrubs, small urban trees, bushes, medium-sized vegetation
Forest/Plantation	Deciduous and coniferous forests, agricultural plantation, urban trees
Water	Lakes, ponds, pools, rivers, dredging lake

Mean building height is computed using the vector DSM rasterized to 1-m cell size. Averages omitting the ground pixels, but including trees, are calculated on a 15-m grid. The same DSM is used to calculate the building to surface fraction, which represents the ratio of building to non-building pixels in a 15-m grid environment.

Aspect ratio is computed using an approach described in detail by Lindberg et al.⁴¹ Using the 1-m raster DSM, the Euclidean distance from each pixel to the nearest wall is calculated. A local maximum algorithm filters the values representing the half-street width (HSW). To receive the corresponding building height to the particular street canyon, the 1-m raster DSM is adjusted using Voronoi polygons (MBH_V) and divided by the HSW as follows: aspect ratio = $\frac{MBH_V}{2 * HSW}$.

Impervious surface fraction and pervious surface fraction are estimated using GIS vector data containing the surface coverage based on a cadastral map of BS. Therefore, percentages of sealed surfaces (including streets, railways, pedestrian ways, motorways, etc.) and nonsealed surfaces (bare soil, parks, forests, water, etc.) are estimated on a 1-m grid. Similar to the other urban morphology parameters, the impervious surface fraction and pervious surface fraction are resampled to 15 m. All rasterizing is done using the Landsat classification image as a geometrical reference to ensure spatial congruence. An overview showing the calculated morphological parameters within the extent of BS is presented in Fig. 2.

2.3.3 Combination of land use/land cover and morphological parameters

LCZ are defined by morphological characteristics and the corresponding thresholds (Table 3). Ideally, a supervised classification based on remote sensing data should result in LULC classes with different morphological behavior throughout different classes.

With the combination of the morphology and LULC classes, the LCZ thresholds, as defined by Stewart and Oke,¹⁷ can be used to characterize the land cover classification.

It needs to be mentioned that LCZ are not intended to be applied on a per pixel scale. Stewart and Oke describe a minimum radius of 300 m as reasonable.¹⁷ Due to the small-scale

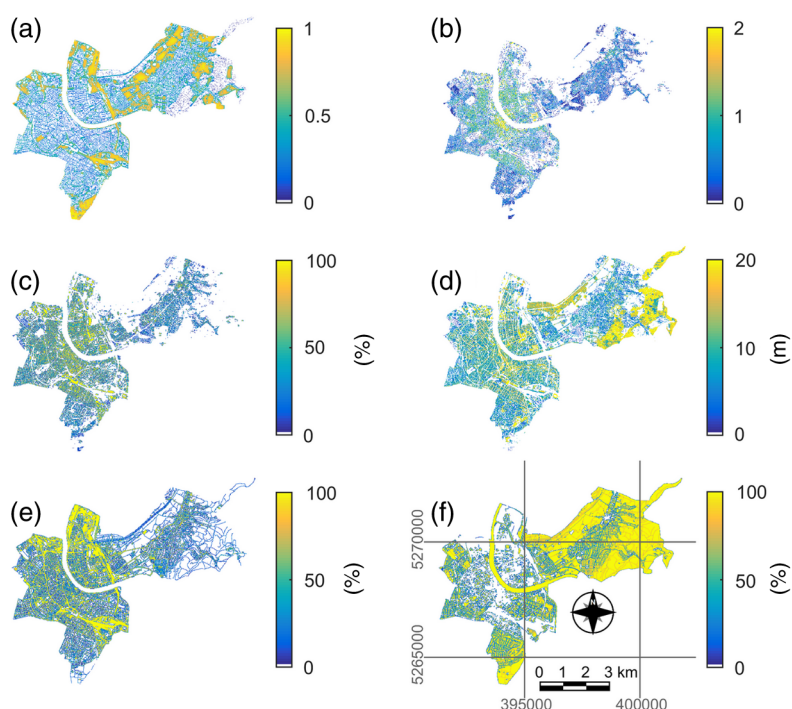


Fig. 2 Morphological parameters [i.e., (a) sky view factor, (b) aspect ratio, (c) building to surface fraction, (d) mean building height, (e) impervious surface fraction and (f) pervious surface fraction] of Basel-Stadt with 15-m resolution and the coordinates in UTM-32N.

characteristics of a typical European city, the proposed radius is not able to depict this heterogeneity. Therefore, the 15-m resolution is retained until potential aggregations are presented at the end of Sec. 4.4.

The workflow and basic steps of the approach are summarized in Fig. 3 as a simple flow chart.

Table 3 LCZ thresholds by Stewart and Oke.¹⁷ Only zones 1 to 10 are shown (built-up zones) and the terrain roughness class criteria is omitted.

Local climate zone	Sky view factor	Mean building height	Building to surface fraction	Aspect ratio	Impervious surface fraction	Pervious surface fraction
LCZ 1 ^a	0.2 to 0.4	>25	40 to 60	>2	40 to 60	<10
LCZ 2 ^a	0.3 to 0.6	10 to 25	40 to 70	0.75 to 2	30 to 50	<20
LCZ 3 ^a	0.2 to 0.6	3 to 10	40 to 70	0.75 to 1.5	20 to 50	<30
LCZ 4 ^b	0.5 to 0.7	>25	20 to 40	0.75 to 1.25	30 to 40	30 to 40
LCZ 5 ^b	0.5 to 0.8	10 to 25	20 to 40	0.3 to 0.75	30 to 50	20 to 40
LCZ 6 ^b	0.6 to 0.9	1 to 10	20 to 40	0.3 to 0.75	20 to 50	30 to 60
LCZ 7 ^c	0.2 to 0.5	2 to 4	60 to 90	1 to 2	<20	<30
LCZ 8 ^c	>0.7	3 to 10	30 to 50	0.1 to 0.3	40 to 50	<20
LCZ 9 ^c	>0.8	3 to 10	10 to 20	0.1 to 0.25	<20	60 to 80
LCZ 10 ^c	0.6 to 0.9	5 to 15	20 to 30	0.2 to 0.5	20 to 40	40 to 50

^aLCZ 1-3: compact high-rise, compact midrise, compact low-rise.

^bLCZ 4-6: open high-rise, open midrise, open low-rise.

^cLCZ 7-10: lightweight low-rise, large low-rise, sparsely built-up, heavy industry.

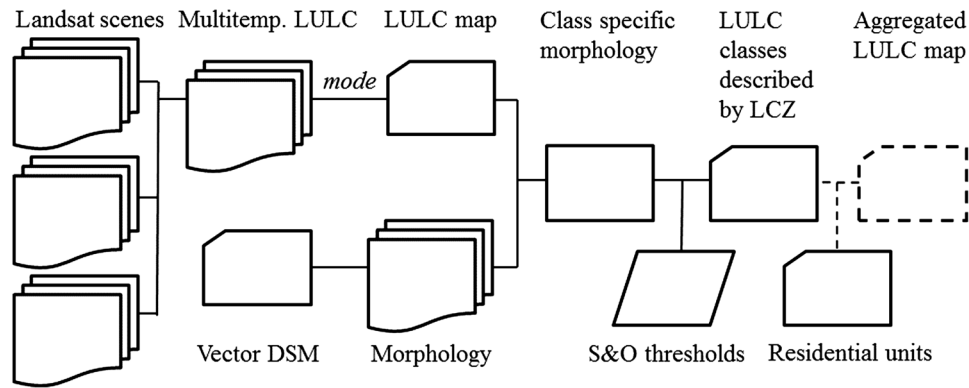


Fig. 3 Flow chart including the basic steps during the data processing.

3 Results

3.1 Accuracy Assessment

The overall accuracy of the classification after the combination and the frequency analysis, estimated using the input ROIs within a confusion matrix, is 83%. The highest amount of incorrectly classified pixels within the ROIs is found in the Urban class. This can be explained with the heterogeneous building types between the historic city center and the suburbs or construction dynamics. The other urban classes reveal accuracies of 76% (Suburban) to 91% (Urban Garden). The two separated industrial classes show substantial overlap with only 56% of Industry/Commercial class pixels and 29% of Rail/Road/Concrete class pixels in the Industry/Commercial ROI field. The latter showed high purity within its ROI with 93% overlap between ground truth ROI and classification. These two classes are nevertheless separated due to the large differences in building to surface fraction and aspect ratio, which is important for roughness class estimation and urban climate studies. The nonurban classes (agricultural, vineyards, forests, and water bodies) show accuracies of almost 100% with Vineyard/Shrub as the exception. This can be explained with the large number of limestone walls and narrow streets within vineyards, misclassified as built-up areas.

Besides the occurrence matrix, visual interpretation using expert knowledge was performed carefully through the whole scene.

To test the benefit of the multitemporal method, the same quality assessment is performed for all individual classification layers and for a second test run without the pan-sharpening. All seven input classifications showed a lower overall accuracy compared to the combined classification with a mean value of 79%. Comparing the pan-sharpening approach with the original 30-m resolution classification, an improvement of 1% in overall accuracy is achieved using the sharpened images. Nonetheless, in most of the built-up classes, the accuracy is improved by up to 4%. Only the class Industry/Commercial revealed better results without the pan-sharpening approach.

Different ways of using the multitemporal data and panchromatic channel (without pan-sharpening) were tested as well but revealed many more unclassified pixels and are, therefore, not further investigated. The Kappa coefficient is not mentioned in this accuracy assessment due to the findings of Pontius and Millones.⁴²

3.2 Land Use/Land Cover Classification

The LULC map shows high levels of detail and, due to the multilayer approach, high robustness. Detailed structures like bridges, airport runways, motorways, or small urban parks are clearly visible (Fig. 4). The distinction between built-up, water, forest, and other natural surfaces worked almost perfectly due to the use of multiple classification layers and therefore a minimization of misclassification. The inner-urban discrimination is much more difficult, due to mixed pixels and the large heterogeneity within urban environments. Nevertheless, the classification map represents the distribution of different urban built-up types with high accuracy.

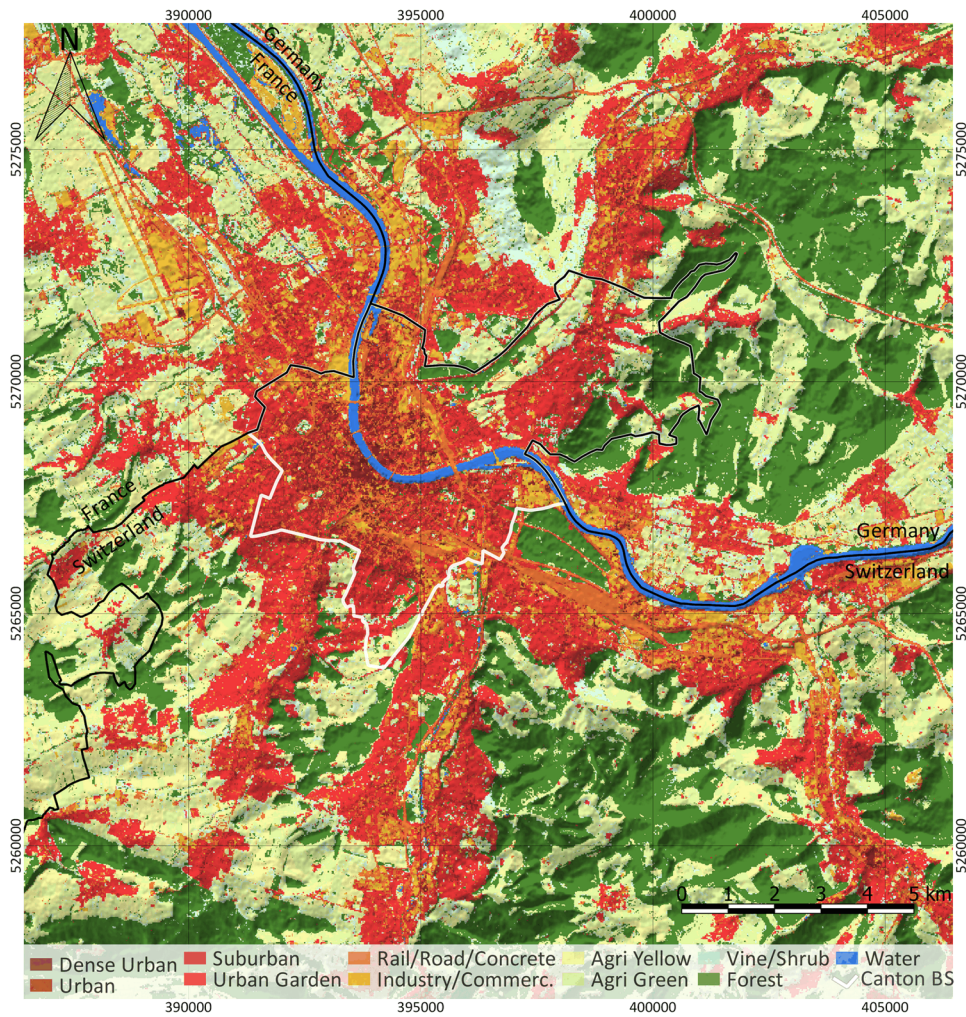


Fig. 4 LULC map of Basel and its surroundings using the modal value of seven individual classifications from 2013 to 2015. The coordinate system is UTM-32N and the pixel resolution is 15 m. The national borders are represented by black lines and the BS border by a white line; a shaded relief overlay using resampled SRTM data depicts the topography. The vegetation represents an overpass of 30 August 2015.

3.3 Morphological Parameters

Histograms describing the frequency distribution of the morphological parameters for every LULC class are shown for the sky view factor [Fig. 5(a)] and the mean building height [Fig. 5(b)]. The histogram displays comparable sky view factors in the urban classes, with increasing tendencies among decreasing urban density. In contrast to the other urban classes, almost all Dense Urban (i.e., old town) pixels have sky view factors below 0.75. These results have been anticipated, but they also show that many of the classes in reality cover a wide range of morphological parameters, which lead to ambiguous assignments of classes.

The mean building height distribution represents the urban structures with medium high buildings in the Urban Dense class, a bimodal distribution due to the typically three to five story buildings in the Urban class and lower mean building height in the Suburban class. The heterogeneous structures within the classes Industry/Commercial and Rail/Road/Concrete with large streets and tower buildings alternated by flat construction halls are represented by the sky view factor (widespread values between 0.2 and 0.9) and the bimodal distribution in the mean building height histogram. The Rail/Road/Concrete class also includes train stations, bridges, and large concrete roofs, such as parking flats. Therefore, the building height distribution also contains values far above street level for this class, which might be unexpected.

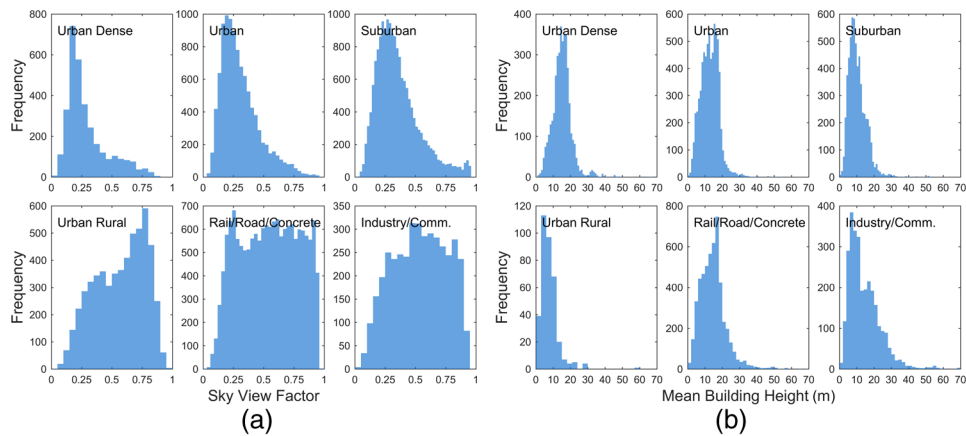


Fig. 5 (a) sky view factor including vegetation and omitting roofs and (b) mean building height including vegetation and omitting streets based on a vector DSM of Basel-Stadt for each built-up class.

Spatial extent, plus mean and standard deviation (σ) of sky view factor, mean building height, building to surface fraction, aspect ratio, and impervious surface fraction are shown in Table 4. The spatial distribution is dominated by the Forest/Plantation class with almost 29%. This class is located mainly on the surrounding hills and provides the city and agglomeration with fresh and cool air due to nocturnal cooling and therefore has an important function for the urban climate system.⁴³

Although essential for urban dwellers and for the cityscape with the historic old town as an important venue, Dense Urban as the smallest class covers only 3.1 km² of the whole study area (0.7%). Suburbs dominate the built-up classes, but the industry classes—due to large industrial zones and extensive railway tracks—are also well represented in the investigation area.

Table 4 Description of the LULC analysis with spatial extent (km² and %) and class specific morphological surface parameters (built-up classes only). The sky view factor is calculated including trees and omitting roofs and the mean building height contains only buildings and trees, without ground pixels. All parameters are based on a resampled DSM (1 m and 3 m for sky view factor) including the Canton Basel-Stadt only.

Class	Total area		Sky view factor ($\pm\sigma$)	Mean building height ($\pm\sigma$) [m]	Building to surface fraction ($\pm\sigma$) [%]	Aspect ratio ($\pm\sigma$)	Imperv. surface fraction ($\pm\sigma$) [%]
	[km ²]	[%]					
Dense Urban	3.1	0.7	0.29 \pm 0.17	15.3 \pm 6.5	46.9 \pm 34.0	1.22 \pm 0.86	46.2 \pm 33.4
Urban	15.4	3.6	0.31 \pm 0.16	12.8 \pm 5.5	32.3 \pm 32.3	0.76 \pm 0.64	41.2 \pm 33.8
Suburban	63.8	15.2	0.36 \pm 0.18	10.3 \pm 5.2	22.0 \pm 28.2	0.46 \pm 0.43	26.3 \pm 29.5
Urban Garden	14.7	3.5	0.57 \pm 0.21	7.6 \pm 5.2	9.3 \pm 17.2	0.21 \pm 0.26	18.6 \pm 25.5
Rail/Road/Concrete	31.7	7.5	0.54 \pm 0.24	14.8 \pm 8.0	22.4 \pm 32.5	0.71 \pm 0.77	60.5 \pm 37.6
Industry/ Commercial	17.3	4.1	0.54 \pm 0.22	14.4 \pm 9.4	38.5 \pm 40.3	0.86 \pm 1.06	50.1 \pm 39.8
Agriculture Yellow	45.9	10.9	—	—	—	—	—
Agriculture Green	74.1	17.6	—	—	—	—	—
Vineyard/Shrub	27.3	6.5	—	—	—	—	—
Forest/Plantation	120.6	28.6	—	—	—	—	—
Water	7.0	1.7	—	—	—	—	—

Table 5 Relation between the LULC classification and LCZ from Stewart and Oke by applying the mean morphological parameters for each class to the LCZ thresholds.¹⁷ The numbers are the respective LCZ types that fit to the given thresholds.

Class	Sky view factor	Mean building height	Building to surface fraction	Aspect ratio	Impervious surface fraction
Dense Urban	1, 3, 7	2, 5, 10	1 to 3, 8	2 to 4, 7	1 to 6, 8
Urban	1 to 3, 7	2, 5, 10	4 to 6, 8	2 to 4	2 to 6, 10
Suburban	1 to 3, 7	2, 5, 10	4 to 6, 10	5 to 6, 10	2 to 6, 10
Urban Garden	4 to 5	3, 6, 8 to 10	~9 ^a	8 to 10	5, 7, 9
Rail/Road/Concrete	4 to 5	2, 5, 10	4 to 6, 10	5 to 6	1 to 6, 8
Industry/Commercial	4 to 5	2, 5, 10	4 to 6, 8	2 to 4	1 to 6, 8

^aNearest LCZ value applied.

Class	LCZ 1	LCZ 2	LCZ 3	LCZ 4	LCZ 5	LCZ 6	LCZ 7	LCZ 8	LCZ 9	LCZ 10
Dense Urb	3	4	4	2	2	1	2	2	0	1
Urban	1	4	3	3	3	2	1	1	0	2
Suburban	1	3	1	2	4	3	1	0	0	4
Urb Garden	0	0	1	1	2	1	1	2	3	2
Rai/Roa/Con	1	2	1	3	5	3	0	1	0	2
Indstr/Com	1	3	2	4	4	2	0	2	0	1

Fig. 6 Affiliation of LULC classes to the LCZ by Stewart and Oke¹⁷ according to the LCZ thresholds. All matches are summed up (maximum = 5, dark gray) and the individual boxes are colored according to the number of matches.

3.4 Combination of Land Use/Land Cover and Morphological Parameters

The combination of the different classification schemes was done using the average morphology of every class and the threshold values given by the definition of Stewart and Oke¹⁷ introduced in Table 3. Most class values fit in several LCZ classes, due to overlapping threshold values, as shown in Table 5.

In the next step, the above table is summarized and evaluated. Figure 6 shows this evaluation with values ranging from 0 (= no matches) to 5 (= fitting to all criteria). Only one class (i.e., Rail/Road/Concrete) matched with exactly one LCZ (i.e., open midrise or LCZ 5) in all criteria. Urban and Urban Garden are the only other classes with explicit matching (four matches) to compact midrise (LCZ 2) and sparsely built (LCZ 9), respectively. The other classes have two matching zones: Dense Urban fits to compact midrise and compact low-rise (LCZ 3), Suburban to open midrise and heavy industry (LCZ 10), and Industry/Commercial to open high-rise (LCZ 4) and open midrise (LCZ 5).

4 Discussion

4.1 Accuracy Assessment

The accuracy assessment using a coherence matrix revealed best results if a combination of multiple land cover classifications is used instead of a single classification. These findings support the simple visual impression. Concerning vegetation cover, agricultural fields or coastal areas influenced by tides, multitemporal analysis can be problematic due to rapid changes. To classify urban structures, which do not change dramatically within 2 years in developed countries, it is useful to consider multiple scenes to handle mixed pixels and complex surface patterns with high accuracy. Falsely classified pixels due to shadowing or drought are minimized and problems with physical similarities of unequal surfaces are reduced in multitemporal analysis.²³

The benefit of using a pan-sharpened image is questionable. The same workflow is applied using 30-m original Landsat 8 data with the same ROIs and the same channel combination. The resulting classification showed slightly lower overall accuracies. Even though a clear quantitative improvement cannot be verified using a coherence matrix, the pan-sharpened classification revealed many more details—such as streets, bridges, or individual buildings—compared to the original 30-m classification. Because these elements represent only a very small amount of the total pixels, the measurable improvement is negligible. Nevertheless, the heterogeneous urban structures showed an improvement using the pan-sharpened image by up to 4% compared to the other classes. The only class that revealed better results in the 30-m classification is Industry/Commercial, which consists of much wider structures like big factories and large streets, which are well represented in a 30-m pixel environment.

4.2 Land Use/Land Cover Classification

The developed LULC classification scheme is based on a classical maximum-likelihood classification using ground truth data. The highly heterogeneous and small-scale structures within an urban environment could only be captured using the higher resolution pan-sharpened data. The main goal of this classification is to differentiate inner-urban structures, which were better resolved using the sharpened images. The use of multitemporal images thereby reduced possible errors and smoothed the results. The differentiation between natural and built-up classes was successful, but the ambitious goal of differentiating inner urban structures explicitly could not be completely achieved. Nevertheless, due to the heterogeneity of urban environments, the results are sufficient and will be used as an input for future urban climate studies.⁴⁴

The presented LULC classification is only a means to an end and the focus of the work is on the combination of any given LULC classification with morphological characteristics. The classification represents the city configuration accurately and the results show reasonable structures mirroring the reality. Micrometeorological differences within the classes defined in the LULC analysis—and therefore a suitable basis for LCZ comparisons—are confirmed by the findings of the BUBBLE-project (2001 to 2002) with nocturnal air temperature differences and differences in the energy balance within various urban environments in Basel.³²

Therefore, the resulting LULC classification serves as an input for subsequent investigations.

4.3 Morphological Parameters

Morphological parameters are an ideal description of the characteristics of any given city. They allow comparisons independent of sun elevation or surface materials. Therefore, cities throughout the world can be compared using the same thresholds according to city structures.

Most of the morphological parameters are well defined and can be computed easily using existing GIS software. One of the most discussed parameters, however, is mean building height. It can be developed in two ways: masking ground pixels and averaging only building pixels; or averaging all pixels including the ground pixels with a value of zero. Problems occur if—for example—a 100-m tall tower surrounded by a large open square is averaged with completely different results depending on which definition is used. Stewart and Oke use the “geometric average of building heights and tree/plant heights.”¹⁷ In this study, the same definition—omitting ground pixels—was used because the aspect ratio, sky view factor, and building to surface fraction represents the above-mentioned issue in detail.

Limitations in developing morphological parameters exist regarding the availability of such datasets globally. The use of freely available SAR data could be a possible solution to derive morphology without the dependence on high-resolution GIS data.⁴⁵

4.4 Combination of Land Use/Land Cover and Morphological Parameters

The use and application of LCZ for future land cover classification is very promising, but problems and limitations are undeniable. In many European cities, the morphological values between visually clear distinguishable classes (e.g., between old town and Grunderzeit area) often vary less than would be required for the LCZ scheme. Therefore, an additional criterion that is based

Table 6 LULC classes allocated to the LCZ classification scheme by Stewart and Oke¹⁷ based on expert knowledge, basic description of the classes and by analyzing the thresholds for morphological parameters.

Class	LCZ by expert knowledge	LCZ by morphological parameter thresholds
Dense Urban	Compact low-rise (LCZ 3)	Compact midrise (LCZ 2) or compact low-rise (LCZ 3)
Urban	Compact midrise (LCZ 2)	Compact midrise (LCZ 2)
Suburban	Open low-rise (LCZ 6)	Open midrise (LCZ 5) or heavy industry (LCZ 10)
Urban Garden	Sparsely built (LCZ 9)	Sparsely built (LCZ 9)
Rail/Road/Concrete	Open midrise paved (LCZ 5 _E)	Open midrise (LCZ 5)
Industry/Commercial	Heavy industry (LCZ 10)	Open high-rise (LCZ 4) or open midrise (LCZ 5)

on expert knowledge could help to increase the discrimination between classes. Another problem is the definition of industrial classes. In Basel, “industry” means, in most cases, pharmaceutical/chemical industry characterized by office and laboratory buildings, which may be classified as open midrise (LCZ 5). Conversely, they are usually surrounded by large silos and huge factories, which clearly belong to heavy industry (LCZ 10). Using remote sensing data, these areas are usually classified well due to the typically bright surface materials installed, but the LCZ scheme cannot capture them precisely. Furthermore, the class Rail/Road/Concrete is not well represented by the LCZ scheme. Here, a combination of classes, proposed by Stewart and Oke¹⁷ themselves,

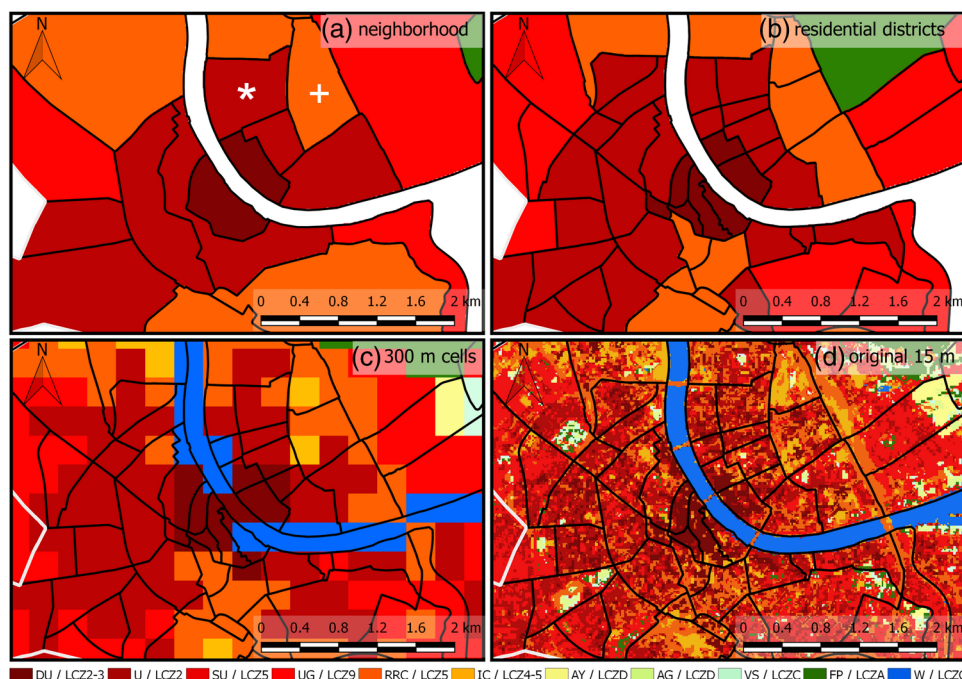


Fig. 7 Possible aggregation (modal value) of the LULC/LCZ using residential units (a and b) and 300-m cells (c). The plotted detail (d) shows the city center and the legend includes the abbreviated class names plus the associated LCZ from Table 6 (right column, with small corrections). The black lines depict the neighborhoods (a) and residential districts (b-d) and the white line delineates the border of the Canton Basel-Stadt. Letters A to G used as suffixes for the LCZ scheme describe the associated land cover types (A = dense trees, C = bush, D = low plants, and G = water).

could solve the problem [e.g., LCZ 5 (open midrise) combined with LCZ E (bare rock or paved)].

The other classes are represented sufficiently by the LCZ scheme, but there is still a need for some adjustments. In Table 6, the results of the semiautomatic LCZ classification are compared with a classification done by expert knowledge, which is strongly influenced by personal opinion. However, the results are promising for future work and useful for comparison between classification schemes.

As mentioned above, LCZ are not applicable on a per pixel scale. One possibility would be to determine the dominating LCZ on a 300×300 m² pixel grid. This procedure results in a large number of mixed pixels and trade-offs, especially in medium-sized cities like Basel [Fig. 7(c)]. A practical approach would be the use of neighborhoods [Fig. 7(a)] or residential districts [Fig. 7(b)], which are administrative units used to collect statistical data. The big advantage of using these spatial units is that the limits are not defined randomly but according to the city structures like ancient city walls or the course of a river. Furthermore, it allows including LCZ in the administrative GIS database of the Canton Basel-Stadt and combining it with statistical data. Disadvantages of using residential units arise from the fact that not all units are as homogeneous as they should be. Urban parks, open squares, or large building complexes disturb average morphology values. For example, the neighborhood Matthaues [white asterisk on Fig. 7(a)] has a substantially lower standard deviation within the mean building height (4.2 m) and the sky view factor (0.13) compared to the adjacent neighborhood Rosental [white plus on Fig. 7(a)] with values twice as high.

5 Conclusion

This study presents the combination of a remote sensing based LULC classification and the LCZ scheme by using morphological parameters. The LULC classification is, therefore, created by a maximum-likelihood classifier using a combination of multitemporal Landsat 8 data. The morphological parameters are derived from a vector DSM and a cadastral map. The morphology is used to characterize the LULC classes and connect descriptive classes with the universal LCZ scheme. This is done using the LCZ thresholds described by Stewart and Oke.¹⁷

The resulting LULC classification is accurate and sufficient for this study in comparison with the “standard” LCZ determination, which leads to many unclassified areas in complex cities with historical city centers and heterogeneous urban structures. The use of multitemporal data enhanced the accuracy and made it more robust with a discrimination of individually misclassified pixels.

The extraction of morphological parameters based on a high-resolution DSM produces excellent results. The analysis showed that the morphology of a city like Basel does not fluctuate substantially. Differences are visible and measurable, but the use of these parameters together with the LCZ thresholds in a strict manner results in large homogeneity and unclassified areas.²⁹ Therefore, the parameters are used to characterize the LULC classes and applied to the LCZ afterward.

This combination offered the possibility of classifying the city according to remote sensing data and assigning them through the morphology to LCZ. Eventually, this could be applied to any LULC classification and serve as a link or a translation between the LCZ and individual classification schemes. Eventually, a possible aggregation of the final zones using residential units is proposed.

Acknowledgments

The authors thank the Grundbuch und Vermessungsamt BS, NASA, GISOR (B. Stern), Natural Earth, and OpenStreetMaps for the free data availability. Special thanks are addressed to Christian Feigenwinter for the link to the URBANFLUXES project,⁴² access to data, fruitful talks, and proofreading; Michael Schmutz and Robert Spirig for data processing and diverse help; Zina Mitrika for important discussions concerning the idea and use of LCZ; Fredrik Lindberg for providing the UMEP software; plus the whole MCR team in Basel for diverse support and the reviewers for their helpful comments. The project leading to this application

has received funding from the European Union's Horizon 2020 research and innovation program under Grant Agreement No. 637519 (URBANFLUXES). The author has nothing to disclose.

References

1. F. Ali-Toudert et al., "Outdoor thermal comfort in the old desert city of Beni-Isguen, Algeria," *Clim. Res.* **28**(3), 243–256 (2005).
2. T. F. Stocker et al., "Climate Change 2013. The physical science basis. Working Group I contribution to the Fifth Assessment Report of the Intergovernmental Panel on Climate Change—Abstract for decision-makers," in *IPCC, C/O World Meteorological Organization, 7bis Avenue de la Paix, CP 2300 CH-1211 Geneva 2, Switzerland* (2013).
3. I. Sandric et al., "Change detection analysis for urban development in Bucharest—Romania, using high resolution satellite imagery," in *Joint Urban Remote Sensing Event (JURSE)*, pp. 1–8, IEEE (2007).
4. R. R. Gillies and T. N. Carlson, "Thermal remote sensing of surface soil water content with partial vegetation cover for incorporation into climate models," *J. Appl. Meteorol.* **34**(4), 745–756 (1995).
5. S. N. Goward et al., "Normalized difference vegetation index measurements from the advanced very high resolution radiometer," *Remote Sens. Environ.* **35**(2), 257–277 (1991).
6. Y. Deng et al., "RNDSI: a ratio normalized difference soil index for remote sensing of urban/suburban environments," *Int. J. Appl. Earth Obs. Geoinf.* **39**, 40–48 (2015).
7. A. Varshney, "Improved NDBI differencing algorithm for built-up regions change detection from remote-sensing data: an automated approach," *Remote Sens. Lett.* **4**(5), 504–512 (2013).
8. H. Xu, "Extraction of urban built-up land features from Landsat imagery using a thematic oriented index combination technique," *Photogramm. Eng. Remote Sens.* **73**(12), 1381–1391 (2007).
9. B.-C. Gao, "NDWI—a normalized difference water index for remote sensing of vegetation liquid water from space," *Remote Sens. Environ.* **58**(3), 257–266 (1996).
10. D. Lu and Q. Weng, "Spectral mixture analysis of the urban landscape in Indianapolis with Landsat ETM+ imagery," *Photogramm. Eng. Remote Sens.* **70**(9), 1053–1062 (2004).
11. R. Powell et al., "Sub-pixel mapping of urban land cover using multiple endmember spectral mixture analysis: Manaus, Brazil," *Remote Sens. Environ.* **106**(2), 253–267 (2007).
12. M. K. Ridd, "Exploring a VIS (vegetation-impervious surface-soil) model for urban ecosystem analysis through remote sensing: comparative anatomy for cities," *Int. J. Remote Sens.* **16**(12), 2165–2185 (1995).
13. C. Y. Sung and M.-H. Li, "Considering plant phenology for improving the accuracy of urban impervious surface mapping in a subtropical climate regions," *Int. J. Remote Sens.* **33**(1), 261–275 (2012).
14. I. Eliasson, "The use of climate knowledge in urban planning," *Landscape Urban Plan.* **48**(1), 31–44 (2000).
15. N. Chrysoulakis et al., "A conceptual list of indicators for urban planning and management based on Earth observation," *ISPRS Int. J. Geo-Inf.* **3**(3), 980–1002 (2014).
16. M.-J. Alcoforado et al., "Application of climatic guidelines to urban planning," *Landscape Urban Plan.* **90**(1–2), 56–65 (2009).
17. I. Stewart and T. Oke, "Local climate zones for urban temperature studies," *Bull. Am. Meteorol. Soc.* **93**(12), 1879–1900 (2012).
18. B. Bechtel and C. Daneke, "Classification of local climate zones based on multiple earth observation data," *IEEE J. Sel. Top. Appl. Earth Obs. Remote Sens.* **5**(4), 1191–1202 (2012).
19. T. Houet and G. Pigeon, "Mapping urban climate zones and quantifying climate behaviors—an application on Toulouse urban area (France)," *Environ. Pollut.* **159**(8), 2180–2192 (2011).
20. U. Fehrenbach, D. Scherer, and E. Parlow, "Automated classification of planning objectives for the consideration of climate and air quality in urban and regional planning

- for the example of the region of Basel/Switzerland,” *Atmos. Environ.* **35**(32), 5605–5615 (2001).
21. I. Stewart and T. Oke, “Classifying urban climate field sites by ‘local climate zones’: the case of Nagano, Japan,” in *Seventh Int. Conf. on Urban Climate*, Yokohama, Japan (2009).
 22. I. Stewart and T. Oke, “Newly developed ‘thermal climate zones’ for defining and measuring urban heat island magnitude in the canopy layer,” in *Eighth Symp. on Urban Environment*, Phoenix, Arizona (2009).
 23. D. Scherer et al., “Improved concepts and methods in analysis and evaluation of the urban climate for optimizing urban planning processes,” *Atmos. Environ.* **33**(24–25), 4185–4193 (1999).
 24. W. Weischet, “Problematisches über die städtische Wärmeinsel und die Notwendigkeit einer Baukörperklimatologie,” *Siedlungsgeogr. Studien* **1**, 407–423 (1979).
 25. W. Weischet, W. Nübler, and A. Gehrke, “Der Einfluss von Baukörperstrukturen auf das Stadtklima am Beispiel von Freiburg iB,” in *Stadtklima, Forschungsgemeinschaft Bauen und Wohnen*, pp. 27–44, Franke, Stuttgart (1977).
 26. U. Fehrenbach, “Analyse und Bewertung lokal- und regionalklimatisch wirksamer Faktoren in der Region Basel,” *Stratus* **6**, 179 (1999).
 27. B. Bechtel, “Multitemporal Landsat data for urban heat island assessment and classification of local climate zones,” in *2011 Joint Urban Remote Sensing Event (JURSE)*, pp. 129–132, IEEE (2011).
 28. B. Bechtel et al., “Mapping local climate zones for a worldwide database of the form and function of cities,” *ISPRS Int. J. Geo-Inf.* **4**(1), 199–219 (2015).
 29. Z. Mitraka et al., “Exploiting earth observation data products for mapping local climate zones,” in *Joint Urban Remote Sensing Event (JURSE)*, pp. 1–4, IEEE (2015).
 30. T. Patterson and N. V. Kelso, “Made with Natural Earth,” 2017, www.naturalearthdata.com (16 December 2016).
 31. MeteoSwiss, “Climate normals Basel/Binningen. Reference period 1981–2010,” in *Federal Office of Meteorology and Climatology MeteoSwiss*, Zurich (2016).
 32. M. W. Rotach et al., “BUBBLE—an urban boundary layer meteorology project,” *Theor. Appl. Climatol.* **81**(3–4), 231–261 (2005).
 33. E. Parlow, R. Vogt, and C. Feigenwinter, “The urban heat island of Basel—seen from different perspectives,” *Die Erde—J. Geogr. Soc. Berlin* **145**(1–2), 96–110 (2014).
 34. Basel-Stadt, *Geoportalkanton Basel-Stadt*, Grundbuch und Vermessungsamt des Kantons Basel-Stadt, Basel-Stadt, Switzerland (2016).
 35. C. A. Laben and B. V. Brower, *Process for Enhancing the Spatial Resolution of Multispectral Imagery Using Pan-Sharpning*, Eastman Kodak Company, Rochester, United States (2000).
 36. Y. Zhang and R. K. Mishra, “A review and comparison of commercially available pan-sharpening techniques for high resolution satellite image fusion,” in *Geoscience and Remote Sensing Symp. (IGARSS)*, IEEE, Munich, pp. 182–185 (2012).
 37. J. D. Paola and R. Schowengerdt, “A detailed comparison of backpropagation neural network and maximum-likelihood classifiers for urban land use classification,” *IEEE Trans. Geosci. Remote Sens.* **33**(4), 981–996 (1995).
 38. A. Asmala, “Analysis of maximum likelihood classification on multispectral data,” *Appl. Math. Sci.* **6**(129–132), 6425–6436 (2012).
 39. A. Knudby et al., “Using multiple Landsat scenes in an ensemble classifier reduces classification error in a stableF nearshore environment,” *Int. J. Appl. Earth Obs. Geoinf.* **28**, 90–101 (2014).
 40. F. Lindberg et al., “UMEP—an integrated tool for urban climatology and climate sensitive planning applications,” in *9th Int. Conf. on Urban Climate (ICUC9)*, Toulouse, France (2015).
 41. F. Lindberg, C. Grimmond, and A. Martilli, “Sunlit fractions on urban facets—impact of spatial resolution and approach,” *Urban Clim.* **12**, 65–84 (2015).
 42. R. G. Pontius and M. Millones, “Death to Kappa: birth of quantity disagreement and allocation disagreement for accuracy assessment,” *Int. J. Remote Sens.* **32**(15), 4407–4429 (2011).

43. E. Parlow, D. Scherer, and U. Fehrenbach, "Klimaanalyse der Stadt Zürich (KLAZ)," *Umwelt-und Gesundheitsschutz der Stadt Zürich*, Abschlussbericht (2010).
44. N. Chrysoulakis et al., "A novel approach for anthropogenic heat flux estimation from space," in *9th Int. Conf. on Urban Climate (ICUC9)*, 20-24 July, Toulouse, France (2015).
45. C. Dubois, A. Thiele, and S. Hinz, "Building detection in TanDEM-X data," in *Proc. of 10th European Conf. on Synthetic Aperture Radar*, pp. 1-4 (2014).

Andreas Wicki is a PhD student with the Research Group of Meteorology, Climatology and Remote Sensing (MCR) at University Basel/Switzerland. He received his BS and MS degrees in geoscience from the University Basel in 2013 and 2015, respectively.

Eberhard Parlow has been head of the Research Group of Meteorology, Climatology and Remote Sensing (MCR) at University Basel and a full professor for meteorology since 1989. He received his PhD in physical geography from University Freiburg/Germany in 1982.